Mon. Not. R. Astron. Soc. **365,** 747–758 (2006) doi:10.1111/j.1365-2966.2005.09789.x

Stars beyond galaxies: the origin of extended luminous haloes around galaxies

Mario G. Abadi,[1]★† Julio F. Navarro,[1,2]‡ and Matthias Steinmetz[3]

[1]*Department of Physics and Astronomy, University of Victoria, Victoria, BC V8P 5C2, Canada*
[2]*Max-Planck-Institut für Astrophysik, Karl-Schwarzschild Strasse 1, Garching bei München, D-85741, Germany*
[3]*Astrophysikalisches Institut Potsdam, An der Sternwarte 16, Potsdam 14482, Germany*

Accepted 2005 October 21. Received 2005 October 12; in original form 2005 August 3

ABSTRACT

We use numerical simulations to investigate the origin and structure of the luminous haloes that surround isolated galaxies. These stellar structures extend out to several hundred kpc away from a galaxy, and consist of stars shed by merging subunits during the many accretion events that characterize the hierarchical assembly of galaxies. Such an origin suggests that outer luminous haloes are ubiquitous and that they should appear as an excess of light over extrapolations of the galaxy's inner profile beyond its traditional luminous radius. The mass profile of the accreted stellar component is well approximated by a model where the logarithmic slope steepens monotonically with radius; from $\rho \propto r^{-3}$ at the luminous edge of the galaxy to r^{-4} or steeper near the virial radius of the system. Such spatial distribution is consistent with that of Galactic and M31 globular clusters, suggesting that many of the globulars were brought in by accretion events, in a manner akin to the classic Searle–Zinn scenario. Luminous haloes are similar in shape to their dark matter counterparts, which are only mildly triaxial and much rounder than dark haloes formed in simulations that do not include a dissipative luminous component. The outer stellar spheroid is supported by a velocity dispersion tensor with a substantial and radially increasing radial anisotropy: from $\sigma_r^2/\sigma_t^2 \sim 2$ at the edge of the central galaxy to $\sim$5 at the virial radius. These properties distinguish the stellar halo from the dark matter component, which is more isotropic in velocity space, as well as from some tracers of the outer spheroid such as satellite galaxies. Most stars in the outer halo formed in progenitors that have since merged with the central galaxy or have been substantially disrupted in its immediate surroundings; very few stars in the halo are contributed by satellites that survive as self-bound entities at the present. Although the stellar spheroid in the simulations is more prominent than in disc-dominated galaxies, many of these features are in reasonable agreement with recent observations of the outer halo of the Milky Way, of M31, and of other isolated spirals, and suggest that all of these systems underwent an early period of active merging, as envisioned in hierarchical models of galaxy formation.

Key words: Galaxy: disc – Galaxy: formation – Galaxy: kinematics and dynamics – Galaxy: structure.

1 INTRODUCTION

Galaxies have no edge. With rare exceptions, the stellar spatial distribution in normal galaxies shows little sign of a sharp outer cut-off, and is reasonably well approximated by density laws that extend smoothly to arbitrarily large radius. Extrapolations of the inner luminosity profile, however, suggest that little light comes from regions of surface brightness much fainter than those traditionally used to define the luminous radii of galaxies ($\sim$25 mag arcsec^{-2}). Perhaps for this reason, together with the obvious observational difficulties inherent in studying regions of low surface brightness, the outer luminous haloes of external galaxies have in the past been regarded as a topic of little more than academic interest.

This impression, however, is rapidly changing, as new data sets start to unveil some unexpected properties of the stellar component that populates the outer confines of galaxies. These developments have been made possible by the development of panoramic

★CITA National Fellow, on leave from Observatorio Astronómico de Córdoba and CONICET, Argentina.
†E-mail: mario@oac.uncor.edu
‡Fellow of CIAR and of the J. S. Guggenheim Memorial Foundation.

digital cameras able to map the light distribution of external galaxies down to unprecedented surface brightness levels, complemented by efficient observational techniques designed to identify and measure radial velocities of outer halo tracers in external galaxies, such as planetary nebulae (PNe; Romanowsky et al. 2003). Finally, the advent of efficient spectrographs in 10-m class telescopes have enabled the measurement of radial velocities of large samples of giant stars throughout the Local Group (Ibata et al. 2004), and dedicated spectroscopic campaigns targeted on giant stars have dramatically increased the sample of tracers in the outer halo of our own Milky Way (Morrison et al. 2003; Battaglia et al. 2005; Clewley et al. 2005).

Likewise, the use of stacking techniques in wide-field surveys such as the Sloan Digital Sky Survey (SDSS) have led to clear detections of a distinct low surface brightness component around both isolated spiral galaxies (Zibetti, White & Brinkmann 2004) as well as central cluster galaxies (Zibetti et al. 2005). The surface brightness profiles of these outer luminous haloes deviate significantly from straightforward extrapolations of the laws that describe the main body of the galaxy, and suggest that estimates of the amount of light in the intergalactic or intracluster medium might need to be revised upward. In the case of clusters, for example, Zibetti et al. (2005) conclude that of the order of 11 per cent of the light in a typical Abell cluster might be in the form of an intracluster luminous component with structural properties distinct from those of the galaxy cluster population and of the central cluster galaxy.

These studies have brought about several unexpected results that challenge some of the accepted premises of the currently accepted galaxy formation paradigm. For example, the kinematics of PNe in the vicinity of several normal ellipticals has been found to be consistent with simple models where such galaxies have no surrounding dark matter halo (Romanowsky et al. 2003, but see Dekel et al. 2005). This result, if confirmed by further studies, would be very difficult to accommodate in the Λ cold dark matter (CDM) scenario, where all galaxies are envisioned to form as a result of the dissipative collapse of baryons within massive dark matter haloes.

In the case of the Local Group, wide-field photometric surveys (and their follow-up spectroscopic campaigns) have modified radically the traditional view of the outer stellar spheroid of the Milky Way and M31. Giant structures interpreted as tidal streams of disrupted or disrupting dwarfs have been identified in both galaxies (Ibata, Gilmore & Irwin 1994; Helmi et al. 1999; Majewski et al. 2003; Ibata et al. 2004), and have solidified the notion that accretion events may play a substantial role in the shaping of individual galaxies. These streams are expected to be short-lived as readily identifiable structures on the sky (Johnston, Spergel & Hernquist 1995; Helmi & White 1999), and, although impressive, they are thought to contribute a relatively small fraction of stars in the halo of these systems. In broad terms, the main characteristics of the outer stellar halo are probably adequately captured by a simple model of a reasonably well-mixed spheroid of stars.

Extensive spectroscopic surveys of giant stars in the outskirts of Local Group galaxies have unravelled some intriguing dynamical properties for the outer halo component. For example, just like PNe around ellipticals, the velocity dispersion of these halo tracers drops significantly in the outer regions of the Milky Way (Battaglia et al. 2005; Clewley et al. 2005). This is a somewhat unexpected result if these galaxies are embedded in extended dark matter haloes, and has prompted renewed interest in the extent and spatial distribution of dark matter in the outskirts of galaxies.

From a theoretical point of view, the interest elicited by outer luminous haloes stems from the fact that, in the currently accepted paradigm, stars are envisioned to form only in the collapsed, high-density regions near the centre of dark haloes, which we identify with the main body of individual galaxies. This prejudice is supported by observations that indicate the need for a threshold gas density below which stars do not form (Kennicutt 1989; Martin & Kennicutt 2001; Schaye 2004), and imply that outer halo stars did not form *in situ* but have been shed from protogalaxies during the merger events that characterize the assembly of galaxies in a hierarchically clustering universe.

In simple words, stars found as far away as, say, 100 kpc from a galaxy's centre originate in satellites whose orbital apocentre was about that large before they spiralled in to merge with the main galaxy. We therefore expect a clear connection between the orbital properties of stars in the outer halo and those of the progenitors that merged to form the present-day galaxy. Unravelling the structure of the outer luminous halo of galaxies may thus be seen as an important step toward unravelling the merging history of individual galaxies. The work presented here is similar in aim to that of Bullock & Johnston (2005) and Diemand et al. (2005), which appeared in preprint form at the same time as ours. Bullock & Johnston adopt a simplified model for the structure of the merging fragments that led to the formation of the stellar halo, whereas Diemand et al. tag 'early collapsing' regions within dark matter only simulations and discuss whether these regions develop structural parameters consistent with stellar haloes. Our work differs from theirs in the adoption of self-consistent modelling of the hydrodynamical evolution of gas, stars and dark matter in a full cosmological context.

In this paper, we analyse the origin and structure of the luminous haloes of galaxies simulated in the ΛCDM scenario. We describe briefly in Section 2 the numerical simulations. The main results of our analysis are presented in Section 3 and discussed in Section 4. We conclude with a brief summary in Section 5.

2 NUMERICAL SIMULATIONS

We analyse a suite of eight numerical simulations of the formation of galaxies in the ΛCDM scenario. These simulations have been analysed in earlier papers, which may be consulted for details on the code used as well as on the numerical set-up (Steinmetz & Navarro 2002; Abadi et al. 2003a,b; Meza et al. 2003, 2005). In brief, each simulation follows the evolution in a ΛCDM universe of a small region surrounding a target galaxy, excised from a large periodic box and resimulated at higher resolution preserving the tidal fields from the whole box. The simulation includes the gravitational effects of dark matter, gas and stars, and follows the hydrodynamical evolution of the gaseous component using the smooth particle hydrodynamics (SPH) technique (Steinmetz 1996). We adopt the following cosmological parameters for the ΛCDM scenario: $H_0 = 65\,\mathrm{km\,s^{-1}\,Mpc^{-1}}$, $\sigma_8 = 0.9$, $\Omega_\Lambda = 0.7$, $\Omega_{\rm CDM} = 0.255$, $\Omega_{\rm bar} = 0.045$, with no tilt in the primordial power spectrum. All simulations start at redshift $z_{\rm init} = 50$, have force resolution of the order of 1 kpc, and mass resolution so that each galaxy is represented, at $z = 0$, with $\sim 125\,000$ star particles.

Dense, cold gas in collapsed regions is allowed to turn into stars at rates consistent with the empirical Schmidt-like law of Kennicutt (1998). The energetic feedback of evolving stars is included mainly as a heating term on the surrounding gas, but the short cooling times in these regions reduce significantly the effectiveness of feedback in curtailing star formation. The transformation of gas into stars thus tracks closely the rate at which gas cools and condenses at the centre of dark matter haloes. As discussed in the references listed in the above paragraph, this results in an early onset of star-forming

activity in the many progenitors of the present-day galaxy present at high redshift. This leads to the formation of a prominent spheroidal component as these progenitors coalesce and merge to form the final galaxy. Gas accreted after the merging activity abates leads to the formation of a centrifugally supported gaseous and stellar disc component clearly present in most of our simulations, although they make up typically only about ∼30 per cent of the final stellar mass of each galaxy.

It is likely that improvements to our feedback algorithms may lead to revisions in the efficiency and timing of star formation in these galaxies. As we discuss below, outer halo stars originate mainly in the merger of the early progenitors, so reducing the efficiency of early star formation should have some impact on the actual prominence of the outer stellar halo component. We expect, however, that reasonable modifications of the star formation algorithm will affect mainly the number, ages and chemical composition of outer halo stars, rather than its dynamical and structural properties, which we expect to depend mainly on the orbital properties of the merging progenitors and on the structure of the dark matter halo host. Indeed, the dynamical and structural properties of the outer stellar haloes are essentially independent of stellar age, suggesting that these properties are less sensitive to the complex astrophysics of star formation and feedback. We therefore focus our analysis on the structure and dynamics of the outer stellar halo in our eight simulations. These target a small range in mass chosen so that at $z = 0$ the galaxies have luminosities and circular speeds comparable to the Milky Way. We summarize the main structural parameters of the dark matter and stellar components of the simulated galaxies in Table 1.

3 RESULTS

Fig. 1 shows, at $z = 0$, one of our simulated galaxies (KIA3; see Table 1) projected on to a box of 540 kpc on a side. The top panels show the dark matter particles (left) and stars (right) within the virial radius ($r_{\rm vir} \approx 270$ kpc, shown by the outer green circle), defined to encompass a region of mean density 100 times the critical density for closure. Dark matter particles are coloured by their local density, while stars are coloured by their age, as described in the caption.

The bottom panels in Fig. 1 separate the stars in two components: '*in situ*' stars that formed in the most massive progenitor (left) and 'accreted stars' that formed in progenitors that merged with the main galaxy (right). Stars labelled as 'accreted' exclude those associated with self-bound satellite systems that survive until the present. These can be seen clearly in the top-right panel of Fig. 1, but are largely absent in the bottom-right panel, except for a sprinkling of stars associated with a young stream recently torn from a disrupting satellite, visible at $x \sim -20$, $y \sim 10$ kpc. Roughly ∼48 per cent of stars (by mass) formed '*in situ*' in this galaxy, compared with ∼44 per cent which make up the accreted component. Satellites contribute a rather small fraction (∼8 per cent) of all stars within $r_{\rm vir}$. These numbers are typical of our simulations, as may be seen from the numbers listed in Table 1.

Fig. 1 illustrates a number of properties of the stellar component common to all of our simulations. In particular, it is important to note that: (i) stars spread as far out as the virial radius of the system (outer circle in the panels of Fig. 1), although they are more highly concentrated than the dark matter halo; (ii) *in situ* stars (bottom-left panel) are responsible for most of the young stars in the main body of the galaxy (note the prominence of the young disc in the bottom-left panel), and are practically absent from the outer halo; whereas (iii) accreted stars (bottom-right panel) make up preferentially the spheroidal component and dominate the stellar budget in the outer regions of the galaxy.

The relative importance of the 'accreted' versus '*in situ*' components at various radii is shown in Fig. 2. Beyond a radius $r_{\rm lum} = 20$ kpc (marked by arrows in Fig. 2) accreted stars dominate in all our simulations. We define $r_{\rm lum}$ as the 'luminous radius' of the galaxy and refer to stars beyond $r_{\rm lum}$ as the 'outer luminous halo' or 'outer galaxy', for short. Our analysis focuses on the structure and dynamics of the outer halo and, consequently, mainly on the properties of the accreted component.

It is also clear from this figure that the outer luminous halo contains a relatively small fraction of the stellar mass of the galaxy; fewer than 15 per cent of all stars are found between $r_{\rm lum}$ and the virial radius. We note that this is considerably larger than the fraction of stars in the halo of the Milky Way (≈1 per cent; Freeman & Bland-Hawthorn 2002), a result of the high rates of star formation at early times during the formation of the simulated galaxies. We stress that our models are not designed to provide a detailed model of the Milky Way; rather they should be seen as an attempt to recognize the various processes at work during the formation of the spheroidal component as well as their relative importance. The properties of the outer spheroid seem structurally independent of the morphology of the central galaxy even though some of our simulated galaxies have a negligible disc component (Meza et al. 2003) while in others a thin disc contributes half of the light (Abadi et al. 2003a,b). In this sense, we feel that scaling our results to the Milky Way's halo is an intriguing and useful exercise. Finally, we note as well that accreted

Table 1. Structural parameters of dark and luminous components of simulated galaxies. $M_{\rm drk}$ and $M_{\rm str}$ are, respectively, the dark and stellar mass within the virial radius, $r_{\rm vir}$, defined to encompass a region 100 times denser than the critical density for closure. $M_{\rm glx}$ is the total mass of stars within the luminous radius, $r_{\rm lum} = 20$ kpc. $M_{\rm sat}$ is the mass of stars in satellites. $M_{\rm out}$ is the mass of stars outside the luminous radius but not in satellites. $f^{\rm acc}_{\rm glx}$ and $f^{\rm acc}_{\rm out}$ are the fractions of accreted stars in the inner ($r < r_{\rm lum}$) and outer ($r > r_{\rm lum}$) galaxy, respectively. Numbers in parentheses indicate the number of particles corresponding to the dark and stellar components, respectively. In all simulations, the high-resolution dark matter particles are 5.67 times heavier than the gas particles at the initial redshift. Each gas particle may spawn up to three star particles, each of about one-third of its current mass.

Label	$r_{\rm vir}$ (kpc)	$M_{\rm vir}$ (10^{11} M$_\odot$)	$M_{\rm drk}(N_{\rm drk})$ (10^{11} M$_\odot$)	$M_{\rm str}$ (10^{11} M$_\odot$)	$M_{\rm glx}(N_{\rm glx})$ (10^{11} M$_\odot$)	$M_{\rm sat}$ (10^{11} M$_\odot$)	$M_{\rm out}$ (10^{11} M$_\odot$)	$f^{\rm acc}_{\rm glx}$	$f^{\rm acc}_{\rm out}$
KIA1	391.53	29.47	25.96 (35851)	3.32	2.36 (66050)	0.47	0.48	0.38	0.91
KIA2	266.41	9.28	7.88 (42344)	1.29	1.04 (112220)	0.15	0.10	0.30	0.95
KIA3	267.57	9.41	7.92 (42529)	1.25	1.02 (107220)	0.10	0.12	0.42	0.96
KIA4	350.05	21.06	17.96 (78275)	2.75	1.91 (167089)	0.51	0.33	0.56	0.94
KIA5	316.30	17.61	15.13 (81263)	2.25	1.68 (177628)	0.35	0.23	0.40	0.96
KIB1	394.00	31.53	27.19 (37550)	3.53	2.60 (69453)	0.55	0.37	0.39	0.93
KIB2	269.59	9.62	8.18 (43941)	1.33	1.04 (115290)	0.17	0.11	0.38	0.97
KIB3	267.83	9.43	7.94 (43941)	1.23	0.97 (100289)	0.13	0.12	0.49	0.95

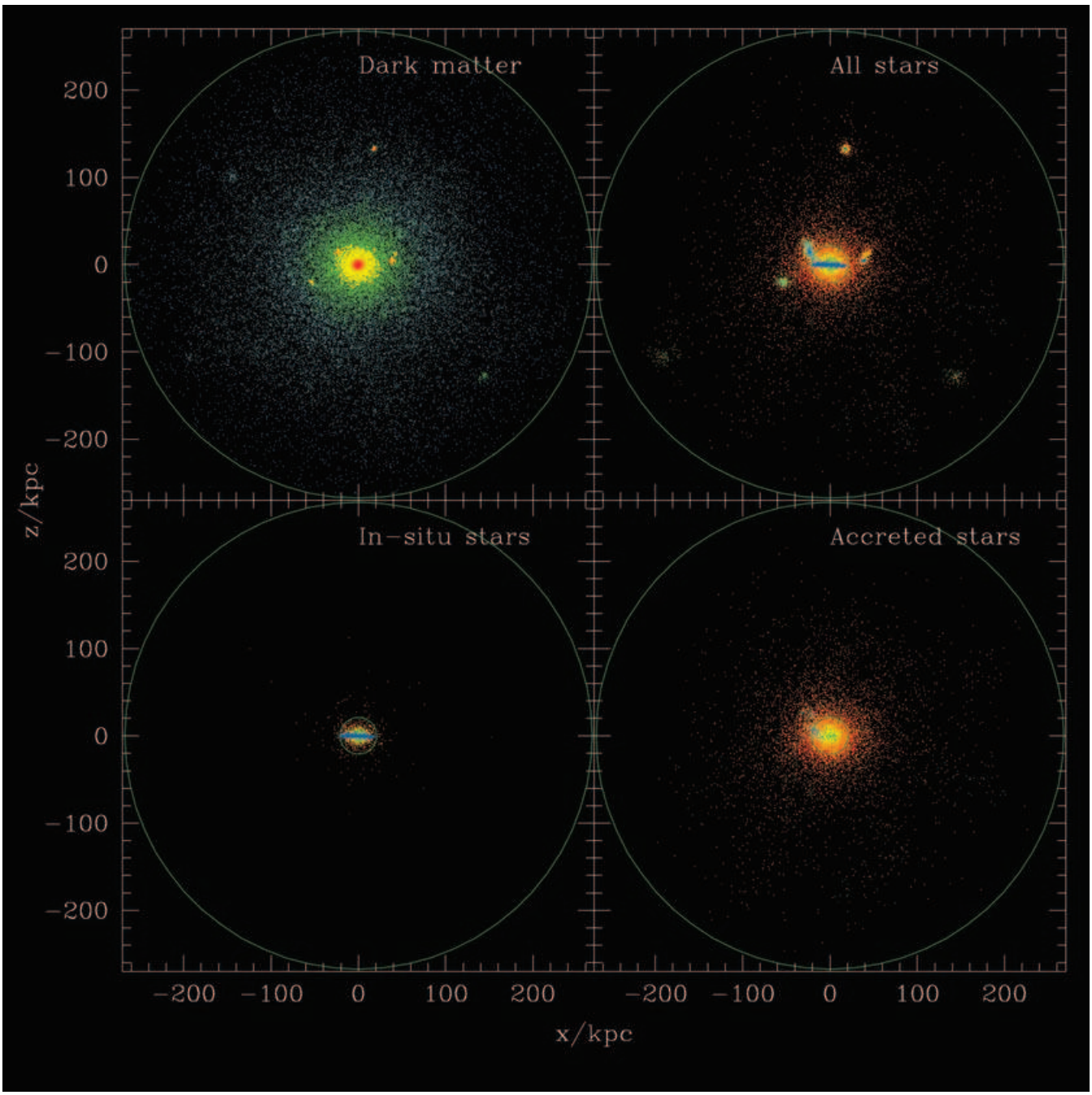

Figure 1. Spatial distribution of the dark matter and stellar component of one simulated galaxy at $z = 0$. Top panels show the dark matter (left) and the stars (right) within the virial radius of the system. Dark matter particles are coloured by their local density, whereas stars are coloured by age (blue, $0.0 <$ age $\mathrm{Gyr}^{-1} < 2.5$; cyan, $2.5 <$ age $\mathrm{Gyr}^{-1} < 5.0$; green, $5.0 <$ age $\mathrm{Gyr}^{-1} < 7.5$; yellow, $7.5 <$ age $\mathrm{Gyr}^{-1} < 10.0$; red, $10.0 <$ age $\mathrm{Gyr}^{-1} < 15.0$). The outer green circle shows the virial radius of the system, and the inner circle shows the radius adopted as the 'luminous radius' of the galaxy. Bottom panels split the stellar component into two different groups: stars formed in the main progenitor of the galaxy (i.e. '*in situ*' stars, left panel) and those contributed by accretion events ('accreted' stars, right panel). The latter group excludes stars in satellites that remain self-bound in the halo of the galaxy.

stars make up a non-negligible fraction of stars in the inner galaxy (i.e. inside $r_{\rm lum}$); we therefore distinguish between 'accreted' and 'outer halo' stars in what follows.

Fig. 3 shows the density profile of the stellar and dark matter components of the simulation shown in Fig. 1. The stellar contribution is split between *in situ* and accreted stars. Note that stars are significantly more concentrated than the dark matter; indeed, they contribute a significant fraction of the total mass within the luminous radius (44 per cent on average for all runs in our series), but they make up a negligible amount of the total mass in the outer regions. Note as well the sharp truncation of *in situ* stars at $r > r_{\rm lum}$; essentially no stars in the outer halo were formed in the main progenitor. This is a natural consequence of the fact that *in situ* star formation proceeds efficiently only in regions of high density. The few *in situ* stars found beyond $r_{\rm lum}$ at $z = 0$ have been torn from the main progenitor during mergers, although Fig. 2 (and the data in

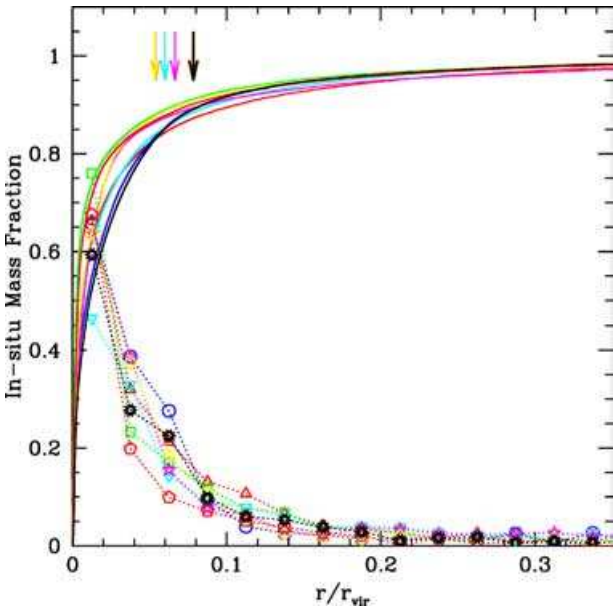

Figure 2. The radial dependence of the fraction of stars formed in the most massive progenitor of the final galaxy (i.e. stars formed *in situ*) is indicated by dotted lines connecting symbols. The thick solid lines indicate the cumulative fraction of stars within the virial radius. *In situ* stars dominate throughout the main body of the galaxy; within the 'luminous radius' of the galaxy, defined to be $r_{\rm lum} = 20$ kpc (shown with arrows), they contribute ∼60 per cent of the stellar mass. Outside $r_{\rm lum}$ the stellar component consists almost exclusively of accreted stars; indeed, fewer than ∼5 per cent of stars in the outer ($r > r_{\rm lum}$) halo formed *in situ*.

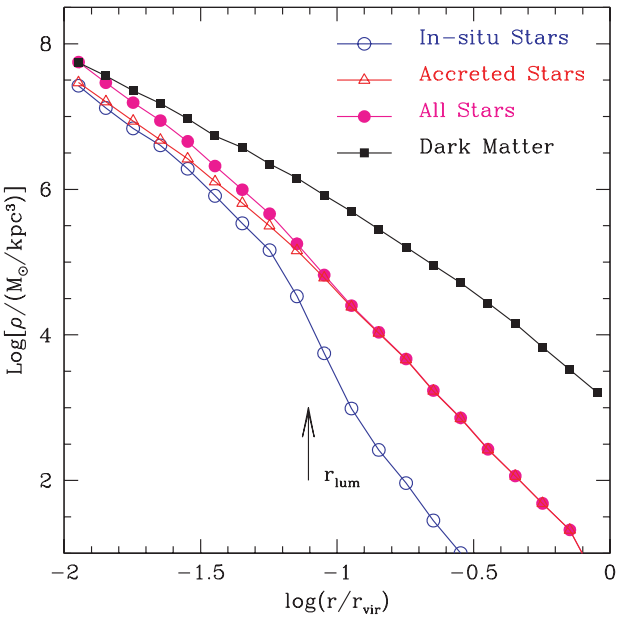

Figure 3. Density profile of stars (circles) and dark matter (squares) in one of our simulations (KIA3), shown in a logarithmic scale. Open circles correspond to the stars formed *in situ*, whereas filled circles correspond to accreted stars. Note that the shape of the density profile of the accreted stellar component is similar to that of the dark matter, and can be adequately fit with a radial law where the logarithmic slope is a power law of radius. See text for details.

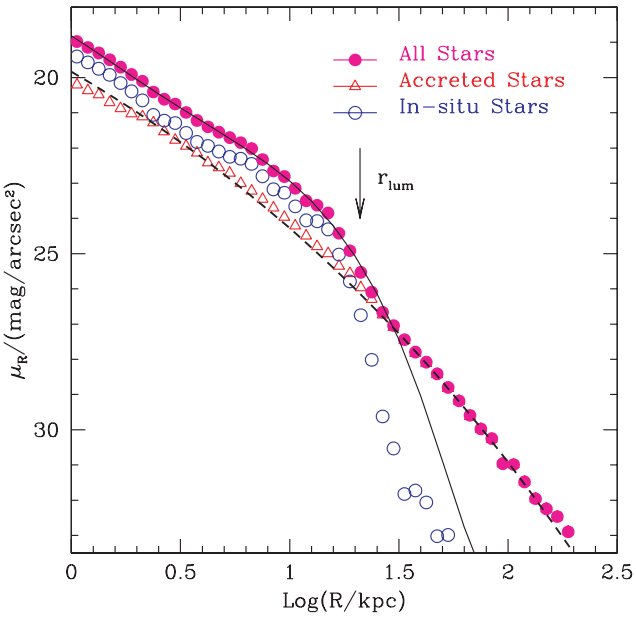

Figure 4. *R*-band surface brightness profile of stars, split between the '*in situ*' and 'accreted' components (run KIA3; see Table 1). The accreted stars dominate outside the luminous radius and appear as an excess of light over a bulge+disc fit to the inner surface brightness profile, which is shown as a solid line. The dashed line shows a Sérsic-law fit to the outer profile of accreted stars. Note that a single Sérsic law (with parameters given in Table 2) reproduces very well the radial distribution of all accreted stars.

Table 1) shows that this is rather inefficient, and that the 'accreted' component dominates the stellar component of the outer halo.

The radius beyond which accreted stars begin to dominate is signalled by an abrupt change in the surface brightness profile of the galaxy, as shown in Fig. 4. Inside the luminous radius, where μ_R is brighter than about 25.5 mag arcsec^{-2}, the surface brightness profile of this galaxy (projected in this case face-on and studied in detail by Abadi et al. 2003a,b) is well approximated by a de Vaucouleurs bulge plus an exponential disc (shown as a solid line). This bulge+disc model is, however, unable to fit the structure of the outer luminous halo, which deviates from the inner profile and appears as a outer luminous 'excess' beyond ∼30 kpc, where the *R*-band surface brightness drops to values fainter than about 26.5 mag arcsec^{-2}.

The outer halo surface brightness profile steepens gradually outwards and is well approximated by a Sérsic law

$$\Sigma(R) = \Sigma_{\rm eff} \exp\left\{-b_n\left[\left(\frac{R}{R_{\rm eff}}\right)^{1/n} - 1\right]\right\} \qquad (1)$$

where $R_{\rm eff}$ and $\Sigma_{\rm eff}$ are, respectively, the radius containing half the light and the surface brightness level at that radius. The surface brightness profile of the outer regions of our simulated galaxies is shown in the left panel of Fig. 5, together with Sérsic-law fits to the outer portion of the profiles.

The Sérsic fit parameters are listed in Table 2. On average, we find $\langle n \rangle = 6.3$ and $\langle R_{\rm eff} \rangle = 7.7$ kpc. The outer luminous halo's surface brightness profile steepens from $\Sigma(R) \propto R^{-2.3}$ at about the luminous radius to $R^{-2.9}$ at $r \sim 100$ kpc and to $R^{-3.5}$ or steeper around the virial radius. The gradually steepening profile of the outer halo characterized by the Sérsic law is reminiscent of the distribution of dark matter, whose density profile also steepens monotonically outward (Navarro et al. 2004). The dark matter profile is, however,

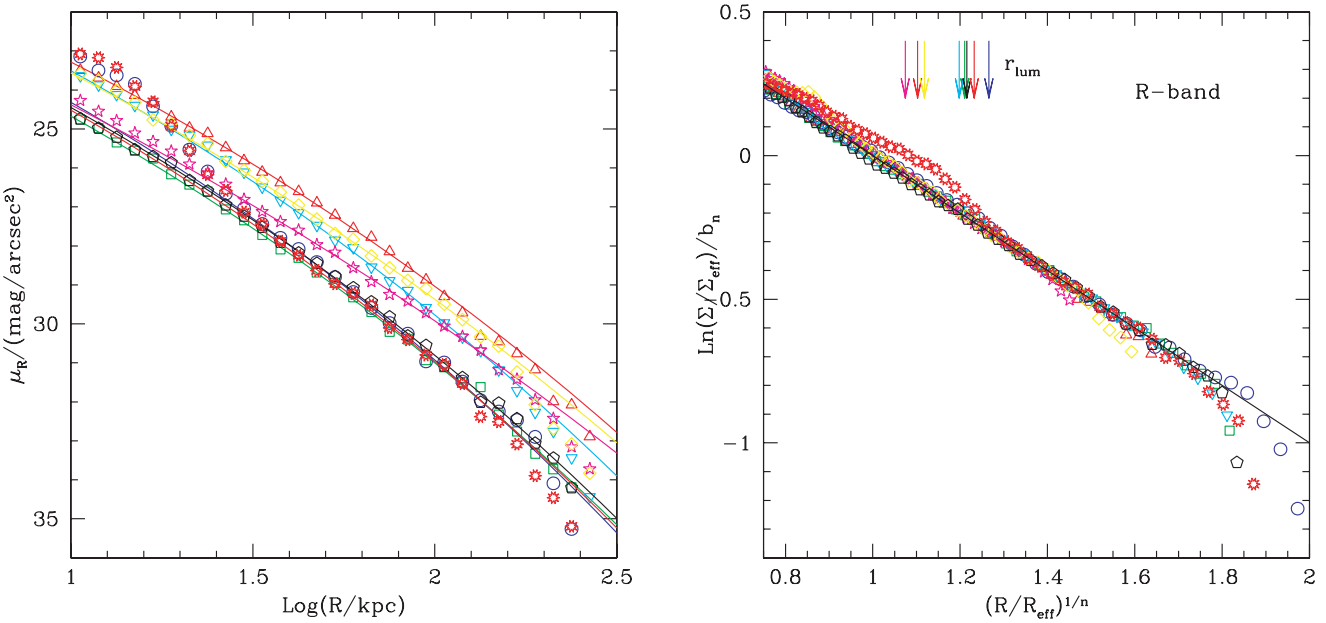

Figure 5. Left: *R*-band surface brightness profile of the outer galaxy ($10 < R/\mathrm{kpc} < 300$) in all of our simulations. Solid lines correspond to the best Sérsic-law fits to the outer regions of the profile ($r > r_{\mathrm{lum}}$) whose parameters are listed in Table 2. Right: same as in the left panel, but profiles correspond only to accreted stars and have been scaled as stated in the axis labels so that Sérsic-law profiles would follow the straight solid line of slope −1. Interestingly, a simple Sérsic law reproduces quite well the radial distribution of accreted stars in all simulations. There is one exception (which shows as a bump in the right panel), associated with the transient effect of an ongoing satellite disruption event.

Table 2. Parameters of Sérsic-law fits to *R*-band surface brightness profile of accreted stars in the outer ($30 < R/\mathrm{kpc} < 130$) galaxy. $L_{\mathrm{tot}}^{\mathrm{fit}}$ is the total luminosity of the Sérsic fit to the outer profile. $L_{\mathrm{tot}}^{\mathrm{acc}}$ is the total luminosity of the accreted stellar component.

Label	n	R_{eff} (kpc)	μ_{eff} (mag arcsec^{-2})	$L_{\mathrm{tot}}^{\mathrm{fit}}$ (10^{10} L$_\odot$)	$L_{\mathrm{tot}}^{\mathrm{acc}}$ (10^{10} L$_\odot$)
KIA1	5.01	12.41	23.62	3.15	3.68
KIA2	6.13	6.05	23.48	0.85	1.03
KIA3	5.73	5.45	22.93	1.10	1.44
KIA4	5.99	6.33	22.36	2.61	3.52
KIA5	8.27	11.06	24.54	1.23	2.07
KIB1	6.95	8.49	23.10	2.57	3.78
KIB2	6.10	6.07	23.30	1.01	1.32
KIB3	5.96	5.62	23.15	0.97	1.90

much less centrally concentrated and its slope is shallower than the stellar halo at all radii. As discussed by Merritt et al. (2005), the dark matter density profile may also be approximated by a Sérsic law, but with a characteristic value of $2 < n < 4$ and much larger effective radii.

The right panel of Fig. 5 shows the surface brightness profiles of the accreted stellar component only for all eight simulations in our series. The profiles have been scaled so that they would all line up along a line of slope −1 if they followed accurately a Sérsic law. All profiles are indeed well approximated by equation (1), with the possible exception of one case where a 'bump' of stars associated with an ongoing satellite disruption event is seen just outside R_{eff} (open starred symbols in the right panel of Fig. 5). This raises the interesting prospect of estimating the total fraction of stars accreted throughout the history of a galaxy simply by fitting its outer profile. As the last two columns of Table 2 demonstrate, the total light contributed by accreted stars is well approximated (to within a factor of ∼2) by the total light of a Sérsic-law fit to the outer luminous halo.

The similarity between profiles suggests that the violent relaxation associated with mergers endows the accreted stellar component with a simple, roughly self-similar structure that is well approximated by a Sérsic law. This process has been studied extensively in the literature, and previous studies have consistently found that the structure of *N*-body merger remnants is quite reminiscent of that of bright ellipticals (see, for example, Barnes & Hernquist 1992 and references therein), which are indeed well approximated by a Sérsic law with $n \gtrsim 4$ (see, for example, Graham & Guzmán 2003 and references therein).

One may think of the accreted stellar component as formed by the overlap of the many 'tidal tails' stripped from the merging progenitors; in this interpretation, the outer luminous halo would just be the superposition of the outer tails stripped from each progenitor during the merger process. This characterization of the accreted stellar component helps to explain the remarkable kinematics of the outer halo shown in Fig. 6. This figure shows the velocity dispersion profile of stars and dark matter, averaged over all simulations after scaling the positions and velocities of all particles to the virial radius and virial velocity of each system. The right panels in Fig. 6 show that the velocity dispersion of the dark matter declines gradually from the centre outwards, and is characterized by a mild radial anisotropy, going from almost isotropic near the centre to $\beta = (1 - \sigma_t^2/\sigma_r^2) \sim 0.3$ in the outer regions. [We use σ_t to denote the tangential velocity dispersion: $\sigma_t^2 = (\sigma_\theta^2 + \sigma_\phi^2)/2$.]

The outer luminous halo, however, shows a much more pronounced radial bias: from $\beta \sim 0.4$ just outside the luminous radius of the galaxy (r_{lum} is on average of the order of $0.06 r_{\mathrm{vir}}$) to about $\beta \sim 0.8$ near the virial radius. This substantial – and monotonically increasing – radial anisotropy may also be understood as a direct

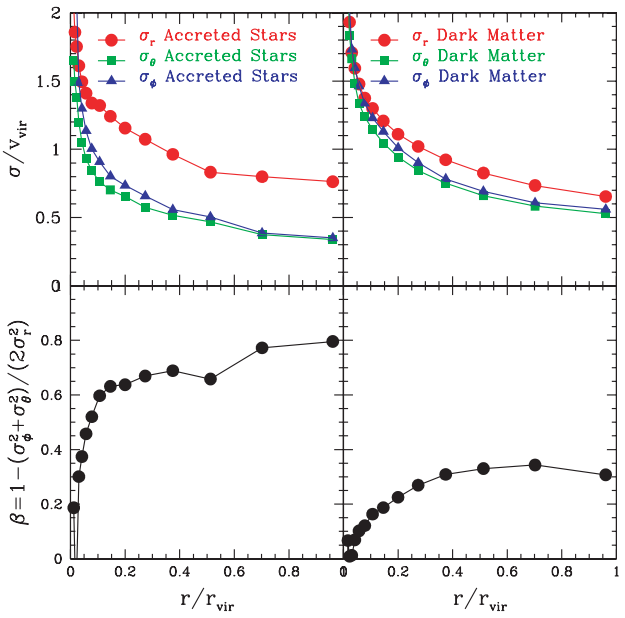

Figure 6. Average velocity dispersion profile of stars and dark matter in our simulations. Averages are computed by scaling all positions and velocities to the virial radius and virial circular velocity of each system, respectively. The rotation axis of the inner galaxy is chosen as the polar axis of the scaling procedure. Particles are then grouped in spherical bins and the spherical components of the velocity dispersion are computed. These profiles are finally averaged over all systems to produce the radial and tangential velocity dispersion profiles plotted here. Right panels correspond to the dark matter component and left panels to the accreted stars. Recall that, on average, the luminous radius is $\sim 0.06 r_{\rm vir}$ in these units. Note that the dark matter velocity dispersion exhibits a mild radial bias; the radial bias is much more pronounced, and monotonically increasing, in the case of the accreted stellar component.

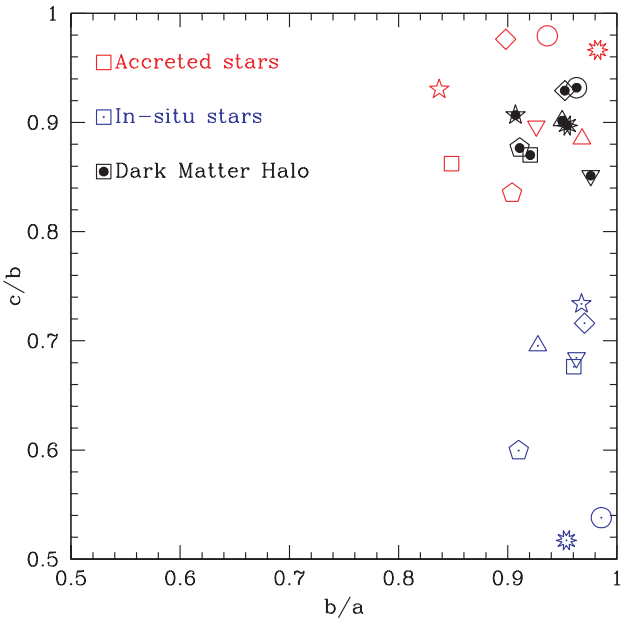

Figure 7. Inertia axial ratios of the dark matter halo, as well as of the accreted and *in situ* stellar components. Axial ratios are computed by diagonalizing the inertia tensor $I_{ij} = \sum m_i x_i x_j$ for all particles of each component within the virial radius of the system. Note that the shapes of the dark matter and accreted components are similar and only mildly triaxial, but that the *in situ* stars are predominantly oblate. This reflects the fact that *in situ* stars have a higher proportion of newly formed stars, which tend to arrange themselves in a disc-like structure (see Fig. 1).

consequence of the tidal disruption process of formation described above. Outer halo stars are typically stripped from merging progenitors during pericentric passages. However, because stars form in high-density regions the stripping of stars operates efficiently only when pericentres are small (and tidal effects are greatest). This occurs typically after dynamical friction has eroded the orbit sufficiently to bring the pericentre of the accreting satellite close to the central galaxy. As a result, outer halo stars are 'launched' into highly energetic orbits with, characteristically, the (small) pericentric radii that accompany the most disruptive tides. Stars able to reach farther are thus typically on more eccentric orbits, leading to the increasing radial anisotropy in the orbits of the outer halo stars seen in Fig. 6.

The formation process of the accreted stellar component is thus qualitatively similar to that of the dark matter halo, where mergers also play a substantial role. It is thus perhaps not surprising that they settle on to similar, mildly triaxial structures, as shown in Fig. 7. For the accreted stars, the average intermediate-to-major axial ratio is $\langle b/a \rangle = 0.91$, whereas the average minor-to-intermediate axial ratio is $\langle c/b \rangle = 0.92$ ($\langle c/a \rangle = 0.84$). This is not too different from the dark matter haloes, which have on average $\langle b/a \rangle = 0.94$ and $\langle c/b \rangle = 0.90$ ($\langle c/a \rangle = 0.84$). We note that the dark matter haloes in these simulations are much rounder than typically found in N-body simulations of CDM halo formation: $\langle b/a \rangle \sim 0.75$ and $\langle c/a \rangle \sim 0.6$ (see, for example, Bailin & Steinmetz 2005). This is the result of the response of the halo to the dissipative assembly of the baryonic component of the galaxy at its centre, which steepens the potential well and reduces the triaxiality of the halo; see, for example, Kazantzidis et al. (2004) and Bailin et al. (2005), and references therein.

The *in situ* stellar component, however, often sports a well-defined rotationally supported disc (see, for example, the lower-left panel of Fig. 1) and its shape is thus well described by an oblate structure with $\langle b/a \rangle = 0.95$ and $\langle c/a \rangle = 0.62$. Although rotation plays little role supporting the accreted component (the mean rotation velocity, $\bar{v}_\phi = j_z/R$, is typically less than one-tenth of the circular velocity at each radius), it is interesting to note that the direction of its angular momentum is well aligned with that of the inner galaxy.

This is shown in Fig. 8, which shows the distribution of the cosine of the angles between the angular momentum of the dark matter halo ($\boldsymbol{J}_{\rm drk}$), the *in situ* stars ($\boldsymbol{J}_{\rm ins}$), and the accreted stellar halo ($\boldsymbol{J}_{\rm acc}$). Although the good agreement between $\boldsymbol{J}_{\rm acc}$ and $\boldsymbol{J}_{\rm ins}$ could have perhaps been anticipated (after all, they are both part of the same stellar system), it is still interesting to note the strong correlation between the rotational properties of the inner galaxy and the dark matter halo. This implies that, although mergers lead to substantial transfer of angular momentum from the stars to the dark halo (Navarro & Steinmetz 1997; Abadi et al. 2003a), this does not alter radically its orientation, so that the spin of the inner galaxy generally ends up aligned with the rotation axis of the surrounding dark matter halo.

It is also of interest to characterize the orientation of the rotation axis relative to the principal axes of the system. Fig. 9 shows the alignment between the galaxy's angular momentum and the minor axis of the dark matter and luminous haloes. No obvious alignment is seen in these panels, suggesting that the rotational properties of the galaxy are, at best, weakly correlated with the shape of the surrounding dark matter (or luminous) halo. We return to possible interpretations of this result in the following section.

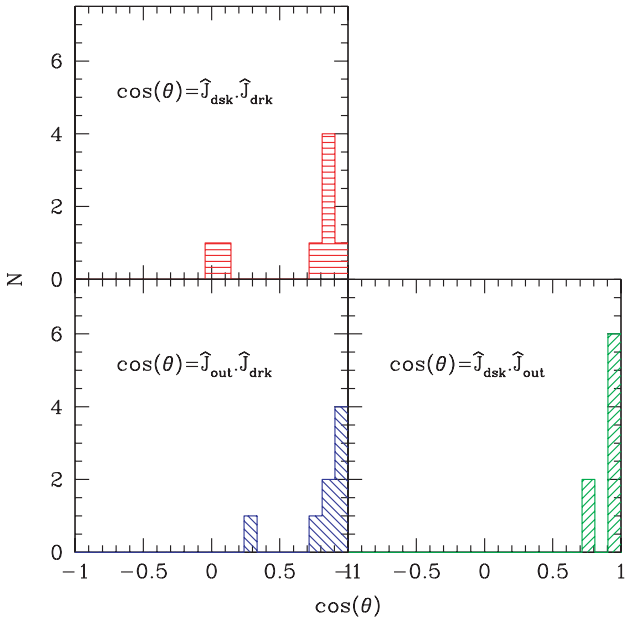

Figure 8. Distribution of the cosine of the angle between the angular momentum vector of the *in situ* stellar component, $\boldsymbol{J}_{\rm ins}$, the accreted stars, $\boldsymbol{J}_{\rm acc}$, and the dark matter, $\boldsymbol{J}_{\rm drk}$. Each of the three different permutations are shown by different shaded histograms, as indicated in the labels of each panel.

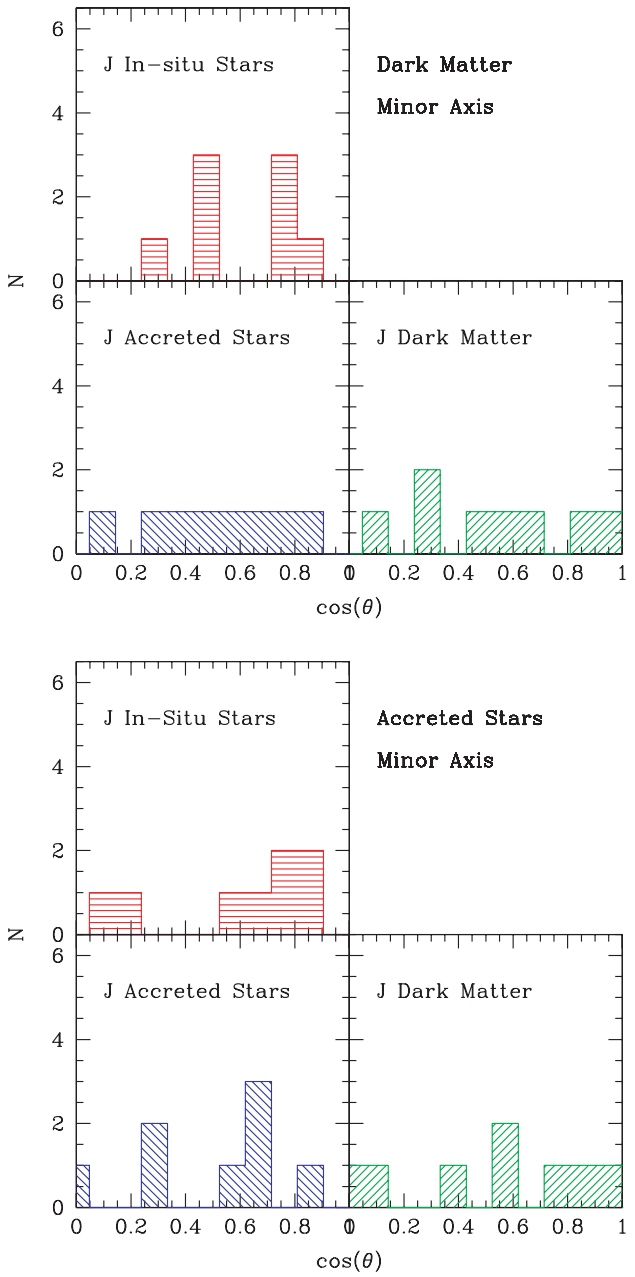

Figure 9. Top: distribution of the cosine of the angle between the angular momentum of *in situ* stars, $\boldsymbol{J}_{\rm ins}$, accreted stars, $\boldsymbol{J}_{\rm acc}$, and the dark matter, $\boldsymbol{J}_{\rm drk}$, and the minor axis of the dark matter. As in Fig. 8, histograms of different shades refer to the various permutations, as indicated in the labels. Bottom: same as the top panel, but for the minor axis of the accreted stellar component.

We end the characterization of the outer luminous haloes of simulated galaxies by comparing the age distribution of stars in the inner and outer galaxy, as well as that of satellites enclosed within the virial radius (Fig. 10). The ages of stars in the outer galaxy ($r > r_{\rm lum}$) differ significantly from those in higher-density regions (such as the inner galaxy or the surviving satellites), where star formation may proceed. The outer halo is populated mainly by older stars, reflecting the fact that the mergers responsible for its formation are more common at earlier times. Interestingly, the distribution of ages of stars in the outer halo is also fairly distinct from that of stars in satellites orbiting within the virial radius. This shows that relatively few stars in the outer halo originate in the 'harassment' of satellites that have survived as self-bound entities until the present (Moore et al. 1996). Most stars in the outer halo come from merger events whose progenitors have long been disrupted (or reduced below the resolution limit) suggesting that the properties of the satellite population may be quite distinct from that of the smooth outer halo.

Although recent hydrodynamical simulations suggest that improving the numerical resolution leads to enhanced survival of the satellite cores (Maccio et al. 2005), this affects mainly the survival of satellites at the faint end of the luminosity function. Most stars in the spheroid are contributed by the largest merger progenitors, which sink and disrupt relatively quickly. This suggests that our conclusion about the distinct nature of halo stars and surviving satellites is robust, although it should be checked carefully by higher-resolution simulations as they become available.

We explore the consequences of these results for the interpretation of observational data in the following section.

4 DISCUSSION

The results presented in the previous section have a number of implications regarding the interpretation of observations of stars in regions far removed from the normal boundaries of typical galaxies. Our simulations suggest that these 'intergalactic stars' (or, more properly, 'extragalactic stars') are a relict of the merging history of each individual galaxy. As such, all galaxies with a past of active merging activity (the majority in a hierarchically clustering scenario such as ΛCDM) should have an outer stellar halo component with properties similar to those described in the previous section.

The outer luminous halo should appear as an excess of light over the extrapolated profile of the inner galaxy. Its structure is characterized by a gradually steepening density profile and by a clearly defined radial anisotropy in the velocity distribution. Outer haloes are rather difficult to detect, because they are – by definition – confined

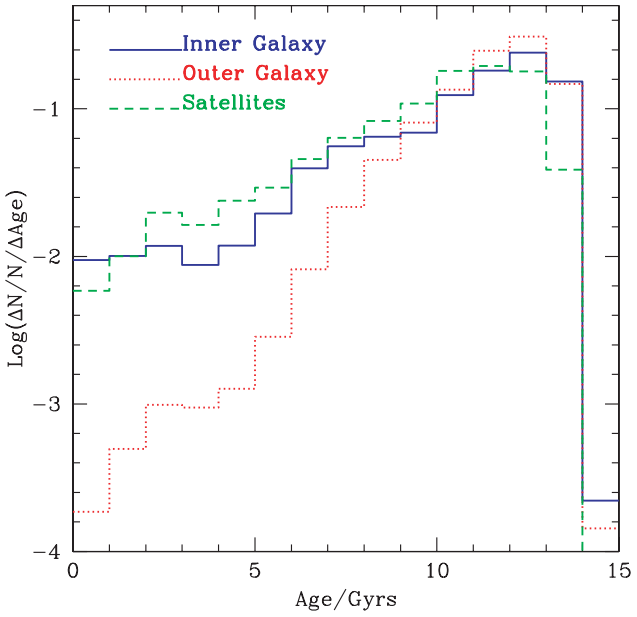

Figure 10. Age distribution of stars in the inner galaxy (i.e. stars within $r_{\rm lum}$, solid blue line), in the outer galaxy ($r > r_{\rm lum}$, dotted red line) and in satellites (dashed green line) enclosed inside the virial radius $r_{\rm vir}$ and averaged over our set of eight simulations.

to regions of very low surface brightness difficult to probe observationally. However, the presence of outer luminous components detached from the properties of the inner galaxy have been recently reported by a number of authors. Following the pioneering work of Sackett et al. (1994), Morrison, Boroson & Harding (1994) and Zheng et al. (1999) among others, Zibetti et al. (2004) have recently reported the statistical detection of a $\rho \propto r^{-3}$ halo of stars in the outskirts of a sample of edge-on disc-dominated galaxies selected from the SDSS.

Encouragingly, this outer halo component is detected as excess light over an extrapolation of the inner disc (see Fig. 4); the halo dominates the minor axis light profile beyond about ∼6 exponential scalelengths, in regions where the r-band surface brightness drops to values fainter than $\mu_r \sim 27.5$. A qualitatively similar result has been derived for M31 through detailed stellar counts by Guhathakurta et al. (2005) and by Irwin et al. (2005), who find that the surface brightness profile along the minor axis 'flattens' relative to an extrapolation of the de Vaucouleurs fit to the inner spheroid at radii beyond ∼20 kpc.

Our simulations provide a compelling interpretation where outer stellar haloes are made up predominantly of stars accreted during previous merger events and, in particular, by the subset which were propelled into highly energetic (and highly eccentric) orbits during the disruption process that accompanies the mergers. Mergers and phase mixing lead then to the formation of a tenuous, distinct stellar component that fills the halo of the galaxy out to the virial radius.

Although we expect them to be ubiquitous, the prominence of these outer luminous haloes is difficult to assess from a theoretical point of view, as it depends critically on the number and timing of merger events, as well as on the fraction of stars present at the time the mergers occur, all of which remain highly uncertain. A number of general inferences are, however, still possible. Late major mergers should propel a proportionally larger fraction of stars into the outer halo, and therefore the relative prominence of this component should be higher in spheroid-dominated galaxies, which are widely regarded as merger remnants. This process should be especially important in systems that have undergone repeated mergers, leading to the expectation that the relative importance of the 'intracluster' stellar component should be highest in clusters with prominent central dominant (cD) galaxies.

In disc-dominated galaxies, where *in situ* star formation is typically still ongoing and mergers are less important, the outer halo is likely to dominate the profile only at large radii, where star formation thresholds prevent the efficient formation of *in situ* stars (Kennicutt 1989; Ferguson et al. 1998; Schaye 2004). The accreted stellar component – to which no such threshold applies – appears then as a distinct outer component, 'flattening' the surface brightness profile in the outer regions, as reported by Zibetti et al. (2004), Guhathakurta et al. (2005) and Irwin et al. (2005).

Quantitatively, we expect the slope of the surface brightness profile of the outer luminous halo to steepen gradually outwards, as dictated by the Sérsic-law fits summarized in Table 2. Given that the average effective radii of the accreted component is 7.7 kpc and $\langle n \rangle = 6.3$, we expect its surface brightness profile to steepen from $\Sigma \propto R^{-2.2}$ at the luminous radius (20 kpc) to $\Sigma \propto R^{-2.9}$ at $r \sim 100$ kpc. This is in reasonable agreement with the results of Zibetti et al. (2004), Irwin et al. (2005) and Guhathakurta et al. (2005). The latter authors, in particular, report that the M31 outer halo may be approximated by $\Sigma \propto R^{-2.3}$ in the range $30 < R < 100$ kpc, slightly shallower than in our simulations, but not inconsistent given the substantial observational uncertainty.

We note as well that the distribution of globular clusters in the Milky Way and M31 is consistent with that of the accreted stellar component in the simulations. With the caveat of small number statistics (only ∼150 globular clusters around the Galaxy and ∼360 around M31 are currently confirmed; see Harris 1996 and Galleti et al. 2004), it is interesting that a Sérsic law with $n \sim 6$ is consistent with the (projected) number density profile of Galactic globulars. This is shown in Fig. 11, where the profile of M31 and Galactic globulars is compared with the Sérsic law that describes the average accreted stellar component in our simulations. We emphasize that the curves shown are not fits, and therefore the general agreement is quite suggestive. A simple interpretation, of course, is that the globular cluster population shares the same 'external' origin as that of accreted stars in our simulations, and that they are thus relicts of the accretion history of each galaxy. [Guhathakurta et al. (2005) note as well that the smooth halo of M31 red giant stars they detect out to ∼150 kpc mimics the distribution of its globular cluster population.] Taken together, the evidence linking globular clusters with accretion events, as envisioned in the classic model of Searle & Zinn (1978), seems quite strong.

In terms of space density, the slope of the accreted stellar component is close to $\rho \propto r^{-3.1}$ near the edge of the luminous galaxy. This is in reasonably good agreement with that inferred from tracers of the stellar halo of the Milky Way in the vicinity of the Sun (see, for example, Saha 1985; Zinn 1985; Morrison et al. 2000). Our simulations imply that the halo profile should steepen gradually with radius and become significantly steeper than r^{-3} in the outer regions. It is interesting to explore the consequences of this gradual steepening for the interpretation of dynamical data in the outskirts of the Milky Way.

Battaglia et al. (2005) report that the velocity dispersion of halo tracers such as blue horizontal branch stars and red giants declines from ∼120 km s^{-1} at the edge of the luminous disc to ∼50 km s^{-1} at ∼120 kpc. These authors argue that the data favour a dark matter halo model with a more steeply declining outer density profile than the extended mass distributions predicted for CDM haloes, such as the

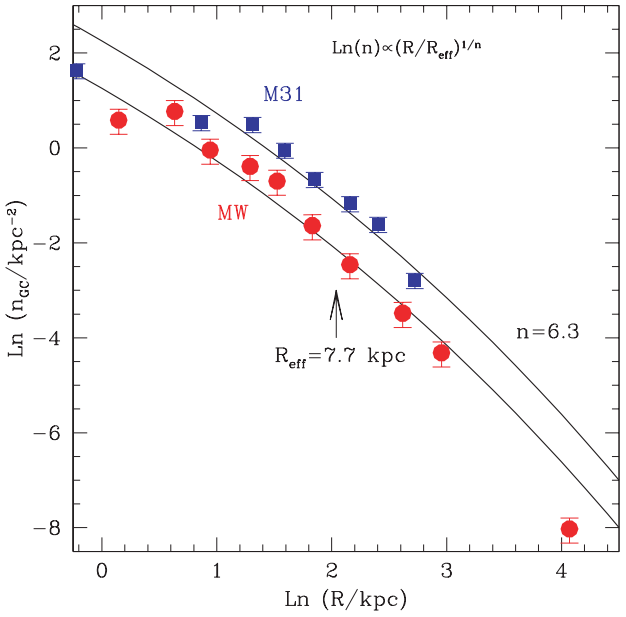

Figure 11. Projected number density profile of globular clusters around the Milky Way (filled circles) and M31 (filled squares), respectively. Data for the 147 Galactic globulars and for the 363 M31 globulars are from Harris (1996) and Galleti et al. (2004). We assume that 100 arcmin = 22 kpc at the distance of M31. We have averaged the distribution of Galactic globulars over several random lines of sight to construct the projected number density profile. Each bin contains 15 and 40 globulars for the Galaxy and M31, respectively, and has Poisson error bars. The two curves are not fits to the data; rather, they illustrate the distribution of accreted stars in our simulations. Parameters for the two Sérsic-law curves are chosen to be the average of the data presented in Table 2 and are vertically scaled to match the data for each galaxy.

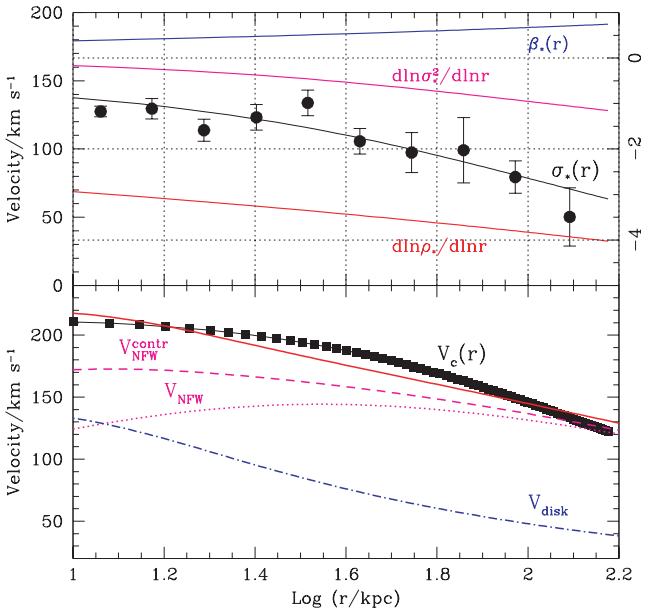

Figure 12. Top: radial velocity dispersion of Milky Way stellar halo tracers (filled circles, from Battaglia et al. 2005). These data are approximated with a simple model where $\sigma_*^2 \propto (1 + r/r_0)^{-2}$, shown by the thin line through the data points. The three other curves (scale at right) illustrate the radial dependence of the right-hand side terms in the Jeans equation (equation 2), derived assuming a Sérsic profile for the tracers. Bottom: solid squares show the total circular velocity of the Milky Way derived from the top panel. The top solid curve shows a fit assuming an (adiabatically contracted) NFW dark matter halo and an exponential disc. The contributions of the dark matter halo (before and after contraction), as well as that of the disc, are also shown. See text for further details.

Navarro, Frenk & White (1996, 1997) (NFW) profile. Neither halo model, however, is completely satisfactory. Extreme radial velocity anisotropy ($\beta \sim 1$) is required to reconcile the data with an NFW halo model although the opposite (i.e. a tangentially anisotropic velocity distribution, $\beta \sim -0.5$) is required for the truncated halo model. The latter seems an unlikely result given that the outer regions of systems assembled hierarchically are typically dominated by radial motions (see, for example, Hansen & Moore 2004 and references therein).

We can use our results to explore the consistency of the velocity dispersion data with CDM haloes. We write the spherical Jeans equation as

$$V_c^2(r) = -\sigma_*^2 \left[\frac{\mathrm{d}\ln\rho_*}{\mathrm{d}\ln r} + 2\,\beta_*(r) + \frac{\mathrm{d}\ln\sigma_*^2}{\mathrm{d}\ln r} \right], \qquad (2)$$

where we have used a $*$ subscript to denote quantities associated with the stellar halo. The terms on the left-hand side of equation (2) may be evaluated by combining the Battaglia et al. data with the assumption that the stellar halo profile may be approximated by a Sérsic law with the (average) parameters given in Table 2. The result of this exercise is shown in Fig. 12.

Interestingly, this simple model predicts a circular velocity near the centre consistent with that measured at the solar circle (~220 km s^{-1}) without tuning (solid squares in the bottom panel of Fig. 12). Further out, the sustained drop in σ_* leads to much lower circular velocities, approaching ~150 km s^{-1} at $r \sim 100$ kpc. This drop in the circular velocity of the system illustrates why the analysis of Battaglia et al. favours a truncated halo. We argue, however, that the data are consistent with an extended CDM halo, and that the velocity dispersion drop places interesting constraints on its total mass.

This is shown in the bottom panel of Fig. 12 by the top thick solid line, which corresponds to an (adiabatically contracted) NFW halo of virial velocity $V_{\rm vir} = 110$ km s^{-1} and concentration $c = 14$ (the average for haloes of this mass in the ΛCDM cosmogony). The halo contributions before and after contraction are shown by the dotted and dashed lines, respectively.

The relatively good agreement with the V_c profile derived from the data implies that, rather than being truncated, the halo of the Milky Way may just be less massive than commonly assumed. The virial mass of the fit shown in Fig. 12 is only $\sim 6.4 \times 10^{11}$ M$_\odot$, and its virial velocity is only one-half of the circular speed at the solar circle. This result is similar to that of Klypin, Zhao & Somerville (2002), who analysed constraints placed by dynamical tracers within the luminous radius of the Milky Way and found that reconciling such data with CDM haloes requires the virial velocity of the dark matter halo to be substantially lower than the rotation speed of the disc. (Their favourite Milky Way halo model has $M_{\rm vir} \approx 10^{12}$ M$_\odot$, which corresponds to $r_{\rm vir} \approx 260$ kpc, and $V_{\rm vir} \approx 130$ km s^{-1}.) We can rephrase this result by stating that the relatively small dark matter contained within the luminous radius of the Galaxy is easiest to accommodate with low-mass halo models, which have the virtue of predicting directly a sharp drop in the velocity dispersion of outer halo tracers. A similar argument was developed by Navarro & Steinmetz (2000), although note the erratum presented in Eke, Navarro & Steinmetz (2001).

It is unclear whether the mass of the halo of the Milky Way is unusually low compared with other spiral galaxies of similar

luminosity, but galaxy–galaxy weak lensing data seem to favour halo masses of the order we find here for late-type L_* galaxies (see, for example, Guzik & Seljak 2002). Also, there is now convincing evidence that the velocity dispersion of satellite galaxies drops at large projected radii so the drop in V_c in the outer regions may actually be a common feature in Milky Way-like galaxies (see Brainerd 2004 for a review).

Turning our attention now to the velocity structure of the outer halo, we recall the pronounced radial anisotropy shown in Fig. 6, and argue that such an effect should not be ignored when interpreting the dynamics of halo tracers in the outskirts of galaxies. As shown by Dekel et al. (2005), accounting for such anisotropies may be enough to reconcile the steeply declining velocity dispersion profiles of PNe around bright ellipticals (Romanowsky et al. 2003) with the presence of massive dark haloes around these objects. The radial anisotropy differentiates dynamically the stars in the outer halo from the dark matter (Fig. 6). It also distinguishes the stellar halo from the population of surviving satellites, which are found to trace rather faithfully the main properties of the dark halo. Indeed, the average anisotropy of the satellite population in our simulations is found to be $\beta \sim 0.45$ (Sales et al., in preparation), closer to that of the dark matter, and certainly less anisotropic than the accreted stellar component.

This dynamical distinction is not surprising, as we find that the smooth stellar halo has little relation with the population of surviving satellites (see Fig. 10). Indeed, few stars in the outer halo may be traced to satellites that survive as self-bound entities until the present. The properties of the stellar halo seem more closely linked to the progenitors of early mergers than to the 'harassment' of the satellite population that survives until the present day.

This result has interesting consequences when applied to the interpretation of the origin of the intracluster light (ICL) component. Zibetti et al. (2005), for example, find that the properties of the ICL in their sample of clusters selected from the SDSS are quite different from those of the cluster galaxy population as a whole. In particular, the ICL is found to be more centrally concentrated than the cluster galaxies and more significantly aligned with the brightest cluster galaxy (BCG) than cluster galaxies. In other words, the ICL seems more intimately related to the central galaxy (BCG) than to the cluster galaxy population. All of these properties are consistent with a scenario where the origin of the ICL is traced to the mergers that led to the formation of the BCG, with a minor contribution from stars stripped from surviving galaxies.

A final item for discussion is the weak alignment between dark halo shapes and angular momentum shown in Fig. 9. At first, this seems to disagree with previous studies, many of which report significant alignment between the rotation axis and the minor axis of CDM haloes (see, for example, Bailin & Steinmetz 2005 and references therein). The issue may be resolved by noting that the shapes of the dark haloes change dramatically when a dissipative baryonic component is included; indeed, in most cases the dark haloes are so nearly spherical that the precise directions of the principal axes are poorly determined. Furthermore, as discussed by Bailin et al. (2005), it appears as if the inner regions of the dark matter halo respond to the assembly of the galaxy by aligning its minor axis with that of the luminous component, but at the same time decouple from the orientation of the halo in the outer regions.

Interestingly, the weak correlations between halo shape and spin that our simulations predict could be tested directly with upcoming weak lensing surveys. Hoekstra, Yee & Gladders (2004) report on a tantalizing correlation between the shape of the luminous galaxy and that of their surrounding matter, but their sample contains a broad mixture of morphological types and a relatively strong contribution from spheroid-dominated galaxies, where the relationship between shape and spin is less clear than in spiral galaxies. Weak lensing analysis applied to spiral-dominated samples should provide further constraints on this topic. This is currently being addressed using large, morphologically segregated samples from the SDSS (Mandelbaum et al., in preparation).

5 SUMMARY

We investigate the origin of stars that populate regions well beyond the traditional luminous boundaries of normal galaxies using numerical simulations of galaxy formation in the ΛCDM cosmogony. Our simulations show that such components are ubiquitous and owe their presence to the many mergers that characterize the early formation history of galaxies assembled hierarchically. These faint stellar haloes extend out to the virial radius of the system, and consist mainly of the overlap and mixing of the many 'tidal tails' shed by merging progenitors during the assembly of the galaxy. Such an origin leads to robust predictions for the dynamics and structure of the outer spheroid that may be contrasted with observation.

(i) The density profile of the accreted stellar component, which dominates the outer luminous halo, is well approximated by a Sérsic-like model where the logarithmic slope steepens monotonically with radius; from $\rho \propto r^{-3}$ near the edge of the galaxy's traditional luminous boundary to r^{-4} or steeper near the virial radius. The shape and concentration of the accreted component are in reasonable agreement with the Galactic and M31 globular cluster population, lending support to the classic Searle–Zinn scenario for the formation of the globular cluster population.

(ii) The accreted stellar component is reasonably well approximated with a mildly triaxial spheroid with average axial ratios $\langle b/a \rangle \sim 0.91$ and $\langle c/a \rangle \sim 0.84$. Rotation plays a negligible role in the support of the accreted stellar component, which is characterized by a strong radial anisotropy in its velocity distribution. This anisotropy grows from the inside out, from $\sigma_r^2 \sim 2\,\sigma_t^2$ in the luminous outskirts of the galaxy to $\sigma_r^2 \sim 5\,\sigma_t^2$ near the virial radius.

(iii) The accreted stellar component is distinct from the dark matter halo as well as from the satellite population, which are typically less concentrated and more isotropic. Most stars in the outer halo formed in progenitors that have since merged with the central galaxy. Only a small fraction of the outer halo stars are contributed through 'harassment' of satellites surviving as self-bound entities until the present.

These properties are in broad agreement with recent observations of the outskirts of spiral galaxies as well as of giant stars in the outer regions of the Milky Way and of M31. In particular, they show that the outer light 'excess' over extrapolations of the inner luminous profile recently reported for M31 and other spirals is a generic feature of galaxies formed hierarchically, and that the decline in velocity dispersion seen in the outer Milky Way halo tracers is consistent with the presence of an extended, massive halo of dark matter (albeit one of perhaps lower mass than commonly assumed). They also imply that the intergalactic stellar component of galaxy clusters may be more intimately related to the central galaxy than to the galaxy cluster population as a whole. These results illustrate ways to unravel the clues to the tumultuous accretion history of individual galaxies contained in the stars ejected beyond their borders.

ACKNOWLEDGMENTS

We acknowledge useful discussions with Simon White, Stefano Zibetti and Vincent Eke. We thank Laura Sales for allowing us to quote some of her results in advance of publication, and Giuseppina Battaglia for providing the data used in Fig. 12 in electronic form. JFN acknowledges support from the Natural Sciences and Engineering Research Council of Canada (NSERC), the Canadian Foundation for Innovation, as well as from the Alexander von Humboldt and Leverhulme Foundations.

REFERENCES

Abadi M. G., Navarro J. F., Steinmetz M., Eke V. R., 2003a, ApJ, 591, 499
Abadi M. G., Navarro J. F., Steinmetz M., Eke V. R., 2003b, ApJ, 597, 21
Bailin J., Steinmetz M., 2005, ApJ, 627, 647
Bailin J. et al., 2005, ApJ, 627, L17
Barnes J. E., Hernquist L., 1992, ARA&A, 30, 705
Battaglia G. et al., 2005, MNRAS, 364, 433
Brainerd T. G., 2004, in Allen R. E., Nanopoulos D. V., Pope C. N., eds, AIP Conf. Proc. 743, The New Cosmology: Conference on Strings and Cosmology. Am. Inst. Phys., New York, p. 129
Bullock J. S., Johnston K. V., 2005, ApJ, submitted (astro-ph/0506467)
Clewley L., Warren S. J., Hewett P. C., Norris J. E., Wilkinson M. I., Evans N. W., 2005, MNRAS, 362, 349
Dekel A., Stoehr F., Mamon G. A., Cox T. J., Primack J. R., 2005, Nat, 437, 707
Diemand J., Madau P., Moore B., 2005, MNRAS, 364, 367
Eke V. R., Navarro J. F., Steinmetz M., 2001, ApJ, 554, 114
Ferguson A. M. N., Wyse R. F. G., Gallagher J. S., Hunter D. A., 1998, ApJ, 506, L19
Freeman K., Bland-Hawthorn J., 2002, ARA&A, 40, 487
Galleti S., Federici L., Bellazzini M., Fusi Pecci F., Macrina S., 2004, A&A, 416, 917
Graham A. W., Guzmán R., 2003, AJ, 125, 2936
Guhathakurta P., Ostheimer J. C., Gilbert K. M., Rich R. M., Majewski S. R., Kalirai J. S., Reitzel D. B., Patterson R. J., 2005, Nat, submitted (astro-ph/0502366)
Guzik J., Seljak U., 2002, MNRAS, 335, 311
Hansen S., Moore B., 2004, MNRAS, submitted (astro-ph/0411473)
Harris W. E., 1996, AJ, 112, 1487
Helmi A., White S. D. M., 1999, MNRAS, 307, 495
Helmi A., White S. D. M., de Zeeuw P. T., Zhao H., 1999, Nat, 402, 53
Hoekstra H., Yee H. K. C., Gladders M. D., 2004, ApJ, 606, 67
Ibata R. A., Gilmore G., Irwin M. J., 1994, Nat, 370, 194
Ibata R., Chapman S., Ferguson A. M. N., Irwin M., Lewis G., McConnachie A., 2004, MNRAS, 351, 117
Irwin M., Ferguson A. M. N., Ibata R. A., Lewis G. F., Tanvir N. R., 2005, ApJ, 628, L105
Johnston K. V., Spergel D. N., Hernquist L., 1995, ApJ, 451, 598
Kazantzidis S., Kravtsov A. V., Zentner A. R., Allgood B., Nagai D., Moore B., 2004, ApJ, 611, L73
Kennicutt R. C., 1989, ApJ, 344, 685
Kennicutt R. C., 1998, ApJ, 498, 541
Klypin A., Zhao H., Somerville R. S., 2002, ApJ, 573, 597
Maccio A. V., Moore B., Stadel J., Diemand J., 2005, MNRAS, submitted (astro-ph/0506125)
Majewski S. R., Skrutskie M. F., Weinberg M. D., Ostheimer J. C., 2003, ApJ, 599, 1082
Mandelbaum R., Seljak U., Kauffmann G., Hirata C. M., Brinkmann J., 2005, MNRAS, submitted (astro-ph/0511164)
Martin C. L., Kennicutt R. C., 2001, ApJ, 555, 301
Merritt D., Navarro J. F., Ludlow A., Jenkins A., 2005, ApJ, 624, L85
Meza A., Navarro J. F., Steinmetz M., Eke V. R., 2003, ApJ, 590, 619
Meza A., Navarro J. F., Abadi M. G., Steinmetz M., 2005, MNRAS, 359, 93
Morrison H. L., Boroson T. A., Harding P., 1994, AJ, 108, 1191
Moore B., Katz N., Lake G., Dressler A., Oemler A., 1996, Nat, 379, 613
Morrison H. L., Mateo M., Olszewski E. W., Harding P., Dohm-Palmer R. C., Freeman K. C., Norris J. E., Morita M., 2000, AJ, 119, 2254
Morrison H. L. et al., 2003, AJ, 125, 2502
Navarro J. F., Frenk C. S., White S. D. M., 1996, ApJ, 462, 563
Navarro J. F., Frenk C. S., White S. D. M., 1997, ApJ, 490, 493
Navarro J. F., Steinmetz M., 1997, ApJ, 478, 13
Navarro J. F., Steinmetz M., 2000, ApJ, 528, 607
Navarro J. F. et al., 2004, MNRAS, 349, 1039
Romanowsky A. J., Douglas N. G., Arnaboldi M., Kuijken K., Merrifield M. R., Napolitano N. R., Capaccioli M., Freeman K. C., 2003, Sci, 301, 1696
Sackett P. D., Morrison H. L., Harding P., Boroson T. A., 1994, Nat, 370, 441
Saha A., 1985, ApJ, 289, 310
Schaye J., 2004, ApJ, 609, 667
Searle L., Zinn R., 1978, ApJ, 225, 357
Steinmetz M., 1996, MNRAS, 278, 1005
Steinmetz M., Navarro J. F., 2002, NewA, 7, 155
Zheng Z. et al., 1999, AJ, 117, 2757
Zibetti S., White S. D. M., Brinkmann J., 2004, MNRAS, 347, 556
Zibetti S., White S. D. M., Schneider D. P., Brinkmann J., 2005, MNRAS, 358, 949
Zinn R., 1985, ApJ, 293, 424

This paper has been typeset from a TEX/LATEX file prepared by the author.